Dual emission and optical gain in PbS/CdS nanocrystals: Role of shell volume and of core/shell interface

Gianluca Sirigu,[1] Andrea Camellini,[1] Haiguang Zhao,[2] Lei Jin,[2] Federico Rosei,[2,3] Alberto Vomiero,[4] and Margherita Zavelani-Rossi[5,6,*]

[1]*Dipartimento di Fisica, Politecnico di Milano, Piazza L. da Vinci 32, 20133 Milano, Italy*

[2]*INRS Centre for Energy, Materials and Telecommunications, 1650 Boulevard Lionel-Boulet, Varennes, Québec J3X 1S2, Canada*

[3]*Institute of Fundamental and Frontier Science, University of Electronic Science and Technology of China, Chengdu 610054, People's Republic of China*

[4]*Department of Engineering Sciences and Mathematics, Luleå University of Technology, 971 87 Luleå, Sweden*

[5]*Dipartimento di Energia, Politecnico di Milano, via Ponzio 34/3, 20133 Milano, Italy*

[6]*Istituto di Fotonica e Nanotecnologie – CNR – Piazza L. da Vinci 32, 20133 Milano, Italy*

(Received 18 April 2017; revised manuscript received 1 August 2017; published 9 October 2017)

Colloidal semiconductor nanocrystals (NCs) emitting simultaneously at two distinct wavelengths are of great interest for multiple applications ranging from ultrasensitive self-calibrating nanoscale sensing to light-emitting diodes and white-light emission. The physical mechanism governing dual emission in core/shell NCs composed of two materials is still under investigation; in particular, the roles of the volume of the shell and of the core/shell interface are not well understood. Here we compare three different PbS/CdS NCs with identical cores, but shells of different thicknesses and different core/shell interfaces. We study photoluminescence (PL) characteristics and ultrafast exciton dynamics with subpicosecond time resolution. We find that dual emission is possible for both thick and thin quantum-confined shells, and for different core/shell interfaces. We show that very thick shells allow the decoupling of shell excitons from core ones and we fully describe the dynamic exciton barrier, connected to efficient shell PL. We discuss the efficiency of shell PL in relation to the properties of the NCs and show that it can give rise to optical gain. Our results provide a comprehensive understanding of the physical phenomena governing dual-emission mechanisms in NCs.

DOI: 10.1103/PhysRevB.96.155303

I. INTRODUCTION

Colloidal semiconductor nanocrystals (NCs) are widely explored as functional materials for applications in photonics [1]. Key properties of NCs are simple synthesis methods, solution processability, high-photoluminescence quantum yield, good photostability, and the possibility to control their electronic structure by engineering their composition, size, and shape. Dual-emitting NCs, which show simultaneous emission at two different distinct wavelengths, are particularly interesting due to unique opportunities offered in applications based on ratiometric fluorescence that include ultrasensitive self-calibrating local temperature sensing [2,3], high selective ionic [4] and pH detection, white-light emission [5,6], white light-emitting diodes (LEDs) [7], and optical switches. Multiple emission originating from a single particle is advantageous, compared to that from multiple particles, because it results in internally referenced signals, reduction of the impact of external factors, higher detection efficiency, and higher probe concentration [3]. Dual emission in NCs has been obtained mainly through two strategies: ion doping, e.g., copper, manganese, or silver [3–5,7–10], and synthesis of specific heterostructures [2,6,11–23]. NC heterostructures can be grown in mainly four different morphologies: multiple-shell NCs [6,11,18,21], tetrapods [12–14,17], dot in rod [11,15], and "giant" or "big volume" shell NCs [2,16,19,20,22,23]. In multiple-shell NCs, it is possible to create a barrier that spatially separates excitons of the first (core) excited state from excitons of the second one (outer shell), allowing for simultaneous radiative recombination from two domains far apart.

Very intriguing is the case of the other configurations, which are composed of only *two* materials (dot core and pods, dot core and rod-shaped shell, dot core and big shell). Here, one emission line originates from core excitons, while the second emission line has been ascribed to trap states [6,17,19], excitons in the pods or in the shell confined by a potential barrier [13,16,20,22,23], or a saturation effect [15,22]. Shell emission seems favored by long pod or rod and large shell volume [12,14,15,19], where usually nonradiative Auger recombination is reduced or suppressed [12,16,18,24]. The most used and studied composition is the CdSe/CdS [12,14–17,23] and very few different compositions have been explored [19,22,25] yet not fully investigated, despite the fact that they are very interesting because they operate in the spectral region close to the infrared. In very few cases rod and shell emission of CdSe/CdS NCs resulted in amplified spontaneous emission (ASE) [15,23] or even laser emission [26], giving additional advantageous properties to the NCs. In this context, it appears that band alignment, interfaces, and shell volume play important roles; nevertheless more studies are needed to achieve a comprehensive understanding of the excited states, charge carrier properties and dynamics, and band alignment dynamic modification, to provide guidelines for the design and synthesis of semiconductor heterostructures composed uniquely of two materials, capable of dual emission.

Here we study PbS/CdS NCs, with identical core and different shell thicknesses and different core/shell interfaces, showing strong or weak dual emission. We analyze the

*Corresponding author: margherita.zavelani@polimi.it

photoluminescence (PL) and probe the electron-hole dynamics with subpicosecond time resolution. The PL from core states is high for all NCs, while that from shell states varies. We find that shell PL can be sustained also with thin quantum-confined shells. We study the efficiency of shell PL and we show its relation with the condition of coupling or decoupling of core and shell excitons. We show that excitons' coupling/decoupling behavior depends on the shell volume and the core-shell interface. Moreover, we observe and describe the evolution of the dynamic hole-blockade effect, study the optical gain, and show that core/shell-decoupled NCs can sustain ASE from shell states. These results provide a deeper understanding of the physics that drives dual-emission processes, highlighting in detail the role of core-shell band alignment and that of the interface, and of the shell volume. This knowledge is very important from a physical point of view as well as for NC engineering.

II. RESULTS AND DISCUSSION

A. Experimental details

We produced different PbS/CdS core/shell NCs with either a "*thin*" or a "*giant*" shell and different core/shell interfaces following the procedures described in detail in the Supplemental Material (SM) [27]. In brief, PbS NCs were obtained by using OLA and OA ligands on $PbCl_2$ and sulfur, respectively, and thermal procedures. Core/shell NCs with thin shell (which we will call core/TS NCs) were synthesized inducing the formation of a thin CdS shell through cation exchange; samples with a "giant" shell were obtained via a subsequent successive ionic layer absorption and reaction (SILAR) procedure at 240 °C under N_2 flow. To vary the core/shell interface the precursor Cd:S stoichiometric ratio was changed from 1:1 to 1:0.8 so as to have an abrupt [22] or alloyed transition [25], that is, a "*sharp*" or a "*graded*" interface. In the following we will refer to core/shell NCs with a giant shell as core/GSS and core/GGS correspondingly for sharp or graded interface. All samples were dispersed in toluene solution. The NCs were previously characterized [22,25] and showed a narrow size distribution. The core is identical for all cases [22,25] with a diameter of ∼1.2 nm. The shell thickness is ∼1.8 nm for core/TS NCs and around 6 nm and 5.5 nm respectively for stoichiometric and nonstoichiometric giant NCs. These dimensions were estimated through transmission electron microscopy images (examples in Fig. S1 in the SM [27]) and inductively coupled plasma-optical emission spectrometry [22,25]. The NCs do not show a spherical symmetry, but rather a tetrahedral shape. The PbS is in the center of the NC; the CdS appears in the zinc-blende (Zb) phase in the inner part of the NC, close to the core, and in the wurtzite phase (Wz) in the outer region.

We excited the samples using a chirped pulse-amplified Ti:sapphire laser generating 100-fs pulses at 800 nm and 1 kHz repetition rate. Pump pulses were generated by frequency-doubling the fundamental wavelength or by a noncollinear optical parametric amplifier using β-barium borate crystals. For pump-probe experiments, they were modulated at 500 Hz by a mechanical chopper and focused in a spot of $(280\times380)\ \mu m^2$ on samples dispersed in toluene. UV-visible probe pulses were produced by white-light supercontinuum generation focusing a part of the fundamental beam in a sapphire plate. Chirp-free differential transmission spectra $\Delta T/T = (T_{on} - T_{off})/T_{off}$, T_{on} and T_{off} being the transmission of the probe through the perturbed and unperturbed sample, were acquired at different pump-probe delays by a fast optical multichannel analyzer operating at full repetition rate. The temporal resolution of the setup is ∼100 fs. For ASE measurements, we produced a thick film by drop cast deposition. In PL and ASE experiments emission was collected by a spectrometer coupled to a bundle of fibers. Samples were kept in toluene solution and all measurements were carried out at room temperature.

B. Photoluminescence measurements

PL spectra of the samples are reported in Figs. 1(a)–1(c), pumping at 400 nm, for different pump fluences, corresponding to different average number of excitons per dot, $\langle N\rangle$. In all three NCs a first broad peak appears in the red region of the spectrum, at around 700–740 nm for core/TS and core/GGS NCs and at ∼660 nm for core/GSS NCs. This is attributed to radiative recombination in the PbS core [22]. A further peak appears at around 485 nm for all the samples, which corresponds to a quantum-confined CdS band edge transition, whose signature can also be observed in the knee of the absorption spectrum [see dashed lines in Figs. 1(a)–1(c)]. This second peak is ascribed to exciton radiative recombination in the Wz-CdS shell [22]. The three samples show PL emission from the shell, yet with completely different weights and behaviors, as we will discuss in the following.

The intensity of core and shell PL as a function of $\langle N\rangle$ is plotted for the three samples in Figs. 1(d)–1(f). We observe that in core/TS NCs, shell PL is very weak and strictly follows the evolution of core PL [see Fig. 1(d)]. This suggests that the core recombination drives the emission processes, and in fact, hole and electron wave functions mostly overlap in the core [19]. The input-output characteristics are linear up to $\langle N\rangle \cong 1$ [see inset of Fig. 1(d)] and sublinear for higher occupancies due to saturation [28] or to a nonradiative Auger mechanism [29]. For $\langle N\rangle$ higher than about 12, the slope of the growth of shell PL is lower than that of core PL (see Fig. S2(a) in the SM [27]). This is ascribed to a saturation of excitons in the core [30] that leads to a higher number of excitons in the shell, adding a new decay Auger channel in the shell. Conversely, in core/GSS and core/GGS NC shells, the PL signal is strong and shows a linear growth for occupancies $\langle N\rangle$ up to 30 or more. This is related to suppression of the Auger effect [29], due to a decrease of the electron-electron interaction in the big shell volume [31], and results in a strong and efficient emission from the shell. The reported data allow further interesting considerations. In core/GSS NCs, the shell emission is observed to be stronger than the core emission even for $\langle N\rangle < 1$ (Fig. S2(b) in the SM [27]). This indicates the presence of shell excitons even for very small occupancies and a decoupling between core and shell excitons, giving rise to independent PL emission. The behavior is slightly different for core/GGS NCs, which show a core PL stronger than that of the shell for $\langle N\rangle$ up to ∼12 (see Figs. S2(c) and S2(e) in the SM [27]), corresponding to saturation of the core. In fact, the 1S state of lead chalcogenides is 8-fold degenerate

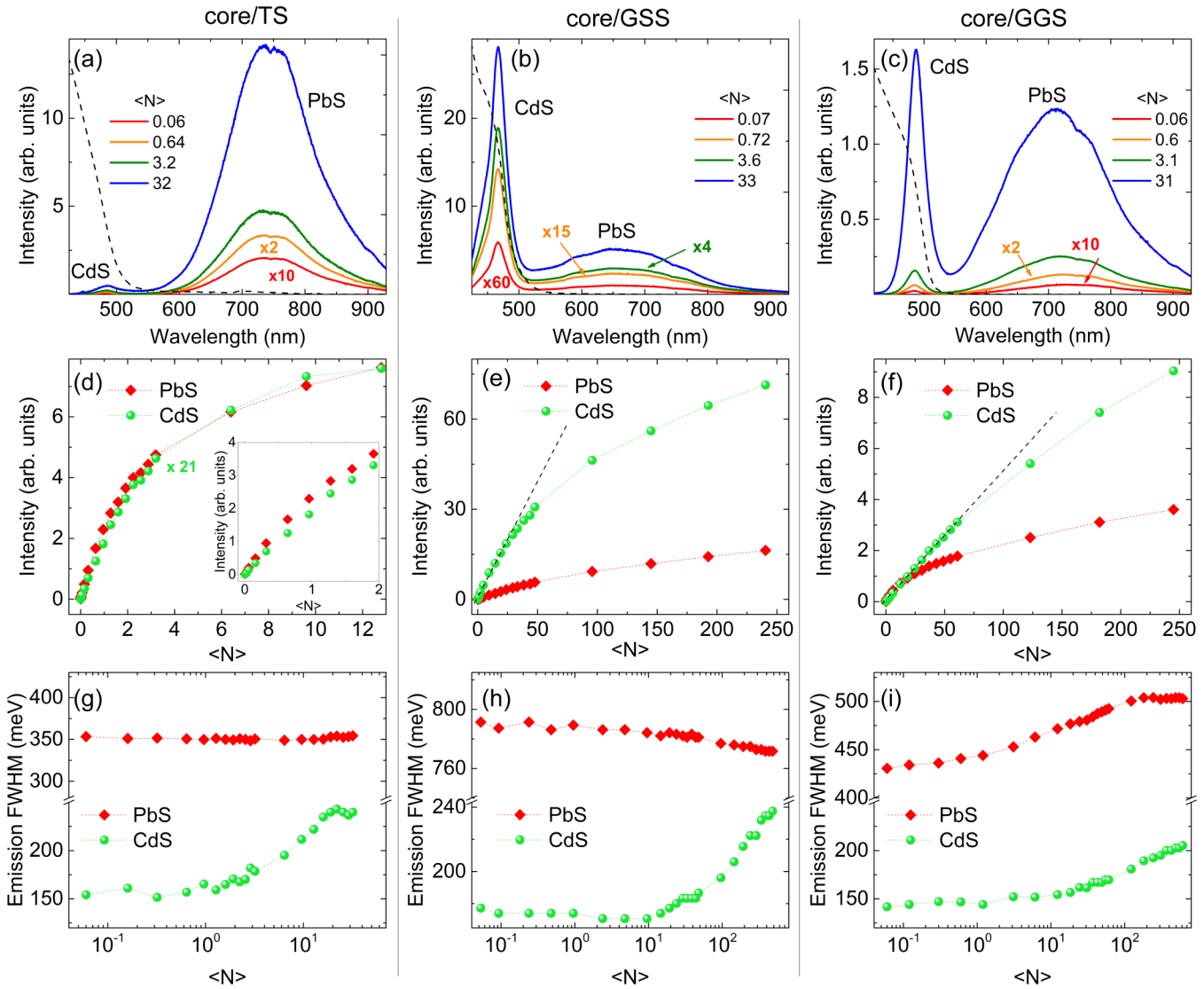

FIG. 1. (a)–(c) PL emission from (a) core/TS, (b) core/GSS, and (c) core/GGS NCs for different $\langle N \rangle$ (dashed black lines are the absorption spectra); (d)–(f) input-output characteristics of time-integrated PL emission at the PbS (red diamond) and CdS (green dots) bands for (d) core/TS, (e) core/GSS, and (f) core/GGS NCs; (g)–(i) full width at half maximum (FWHM) of time-integrated PL spectra for different $\langle N \rangle$ at the PbS (red diamond) and CdS (green dots) bands for (g) core/TS, (h) core/GSS, and (i) core/GGS NCs.

and therefore saturates at $\langle N \rangle = 12$ according to the Poisson distribution of excitons [30]. For $\langle N \rangle$ higher than 12 shell PL is more intense than core PL, which shows saturation, and grows independently from core PL. The PL signal from the shell shows a linear trend for very high occupancies up to ~60. Core/GSS and core/GGS NCs have similar shell volume, but different core/shell interface, so the more efficient shell PL of core/GGS NCs is ascribed to the reduction of the sharpness of the core/shell interface, which prevents the "phonon bottleneck" effect [29,32] and thus explains the reduction of Auger processes.

The relation between core and shell emissions can also be monitored by analyzing the PL lineshape. The full width at half maximum (FWHM) of time-integrated PL spectra as a function of $\langle N \rangle$ is shown in Figs. 1(g)–1(i). In core/TS NCs the line shape of the PbS emission remains almost unchanged in the whole range of $\langle N \rangle$ [Fig. 1(g)] and corresponds to single exciton PL, as we cannot detect biexciton emission, which is much faster than the single-exciton one (with time constants of ~95 ns and ~1.4 μs, respectively [22]). Conversely, upon increasing $\langle N \rangle$ the narrow CdS emission profile remains constant for very low occupancies, then broadens (by ~80 meV) and slightly redshifts (by ~27 meV) for $\langle N \rangle$ greater than 1 and smaller than ~12 [see also Fig. S3(a)], while for higher $\langle N \rangle$ values it remains fixed. Through time-integrated PL only emission processes with comparable lifetimes can be recorded, therefore the observation of the line broadening on the red side of the CdS single exciton peak indicates the presence of radiative attractive biexcitons [33,34] with lifetime comparable to the single-exciton decay time constant (~3 ns) [22]. In addition, the shell PL broadening for $\langle N \rangle$ higher than 1 indicates that even only one exciton in the core generates an electric field that shifts the energy levels of the heterostructure. This effect grows with $\langle N \rangle$ up to the core saturation, which appears at $\langle N \rangle \cong 12$, consistently with previous observations. In giant NCs, we observe a

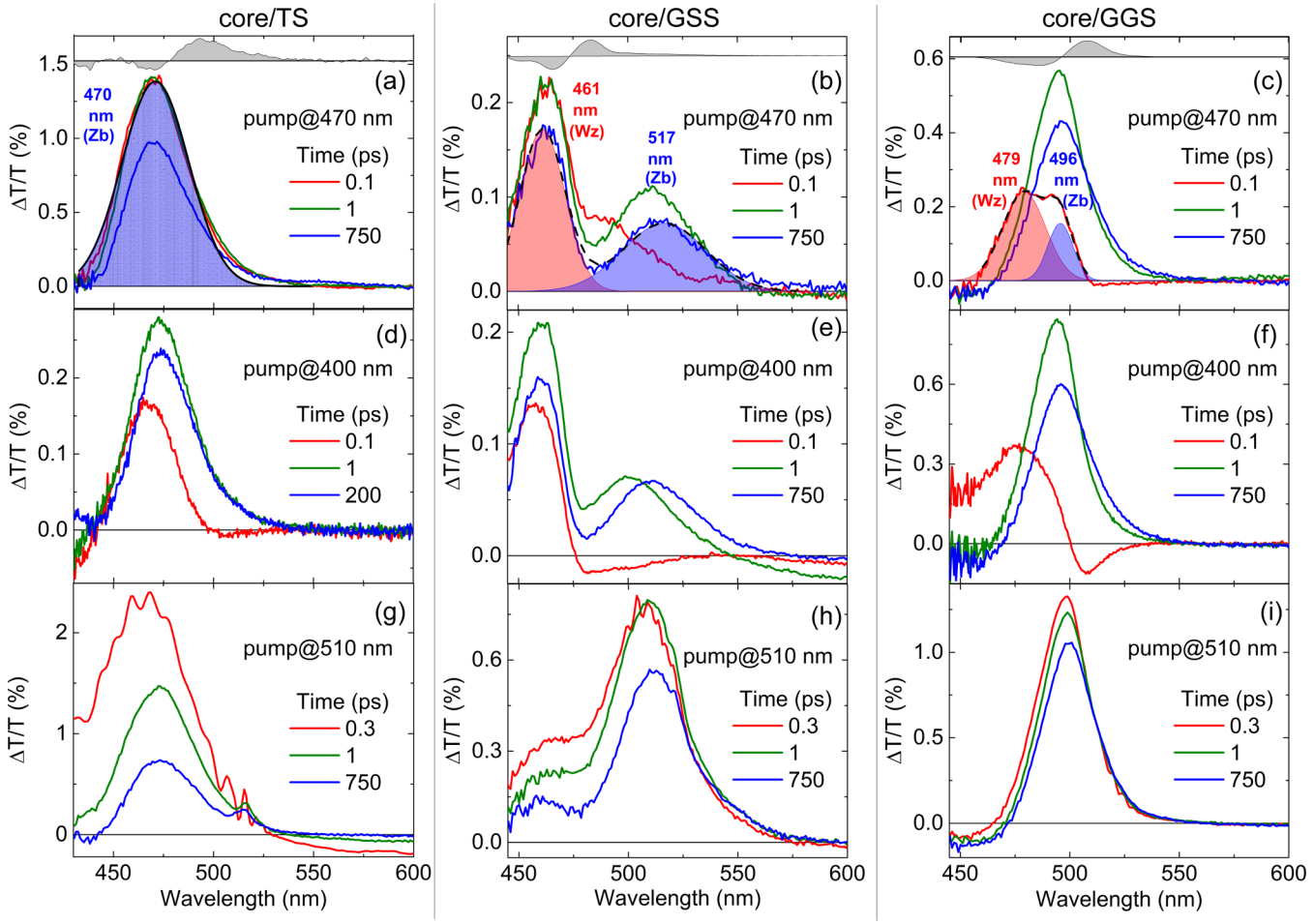

FIG. 2. $\Delta T/T$ spectra at different probe delays for [(a), (d), (g)] core/TS, [(b), (e), (h)] core/GSS, and [(c), (f), (i)] core/GGS NCs, pumping at [(a), (b), (c)] 470 nm, [(d), (e), (f)] 400 nm, and [(g), (h), (i)] 510 nm, with $\langle N \rangle = 0.2$. The time delay is as follows: red lines, 0.1 ps [except in (e) and (f), where it is 0.3 ps]; green lines, 1 ps; blue lines, 750 ps [except in (c), where it is 200 ps]. In (a), (b), (c) the black dashed lines are the fits of the PBs at 100 fs time delay with the respective Gaussian components (red and blue areas) and the gray areas are the second derivatives of the linear absorption of the NCs.

different trend with two main features: changes in the line shape of CdS emission appears only once core saturation is attained, for $\langle N \rangle$ higher than ∼12, and the broadening grows monotonically [by 60–70 meV; Figs. 1(h) and 1(i)]. In core/GGS NCs we also observe a redshift (Fig. S3(e) in the SM [27]). These behaviors are consistent with state filling of higher-lying energy states and with state filling of the lower-energy Zb-CdS band-edge states from which excitons can recombine radiatively. The broadening cannot be assigned to radiative biexciton recombination because the linear increase of the intensity indicates a bulklike behavior of the CdS emission; therefore the high e-h pair binding energy and the large exciton spatial extension prevent the formation of biexcitons [23]. Figure 1(i) shows that in core/GGS NCs the FWHM of the PbS emission increases for $\langle N \rangle$ higher than about 0.4. We ascribe this to biexciton recombination in the core as in this case we can expect a lengthening of biexciton lifetime due to the smoothed core/shell interface [32,35]. This can make biexciton emission visible in time-integrated PL measurements, and the PL blueshift [shown in Fig. S3(f)] indicates the repulsive nature of the biexcitons, which is common in type-II or quasi-type-II band alignment [23,34]. Altogether these observations confirm that in core/TS NCs the shell PL is strictly related to core processes and that the shell cannot accommodate large numbers of excitons, while in giant NCs a large number of excitons can stay in the shell giving rise to processes independent of the core ones.

C. Transient transmission measurements

Transient transmission experiments with ∼100-fs time resolution allowed us to gain insight into the exciton dynamics underlying dual emission. We performed pump-probe experiments with the pump photon energy tuned at different values around the CdS band gap and a white-light probe beam, extending from 420 to 600 nm. The $\Delta T/T$ spectra for a low number of excitons ($\langle N \rangle = 0.2$) recorded at various pump-probe delays are plotted in Fig. 2, while some related temporal dynamics are plotted in Fig. 3. Such low $\langle N \rangle$ was chosen to avoid multiexciton effects. In Figs. 2(a), 2(d), and 2(g) we observe the behaviors of core/TS NCs. We first tuned the pump at 470 nm to promote excitons directly at the band edge of CdS, to avoid thermalization effects or possible high-energy trap states. In this condition, in Fig. 2(a), the

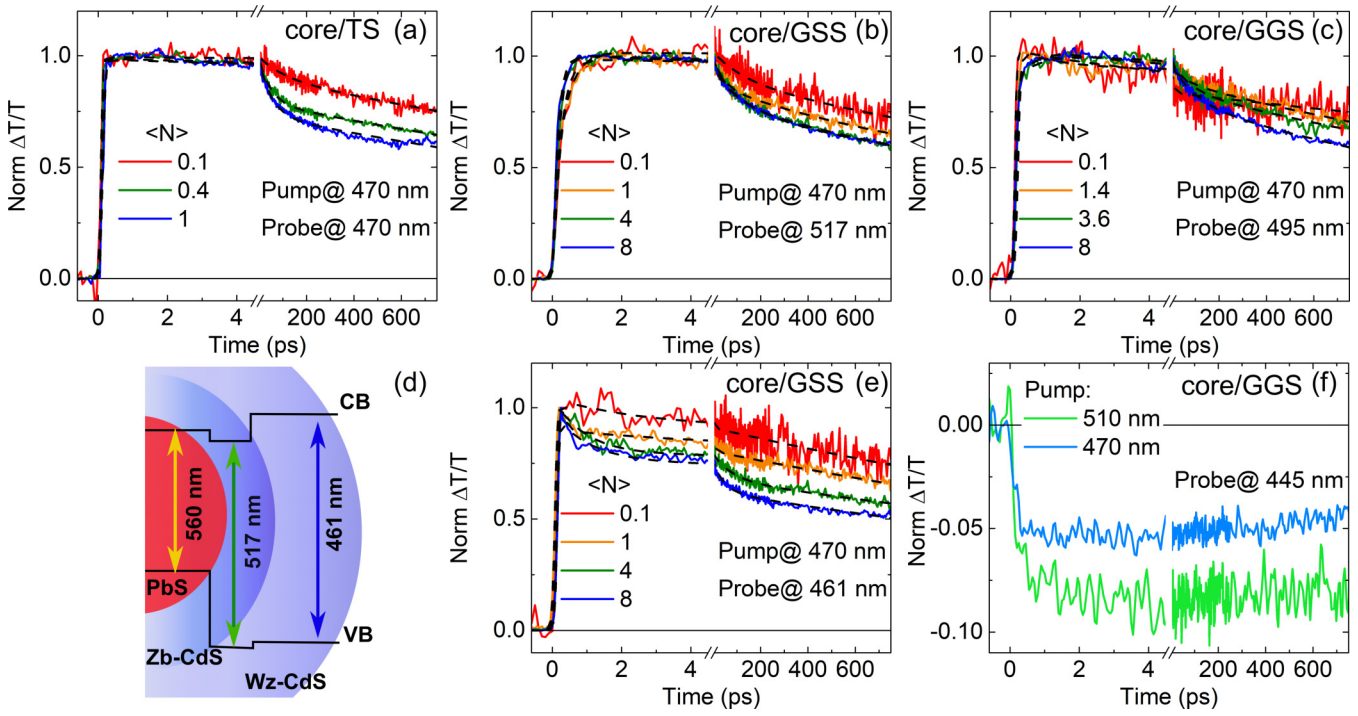

FIG. 3. (a), (b), (c), (e) Normalized $\Delta T/T$ dynamics pumping at 470 nm for different $\langle N \rangle$ for (a) core/TS NCs, (b), (e) core/GSS NCs, and (c) core/GGS NCs at the maximum of the PBs (probe wavelength at 470, 517, 461, and 495 nm respectively). Black dashed lines are the multiexponential fits to the data. (d) Sketch of the energy diagram of core/GSS NCs (spherical symmetry is used for simplicity but does not correspond to real NC shape [22,25]). (f) $\Delta T/T$ dynamics for core/GGS NCs pumping at 510 nm (green line) and 470 nm (light blue line) and probing at 445 nm, normalized at the PB peak ($\langle N \rangle = 1.5$).

$\Delta T/T$ spectrum presents a single positive band corresponding to the photobleaching (PB) of the CdS (its position corresponds to the negative peak of the second derivative peak of the absorption spectrum [36]), which forms in less than ~100 fs and decays very slowly, over the ns time scale that we can probe, with a time constant of few ns [Fig. 3(a)]. Pumping with high-energy photons (at 400 nm) [Fig. 2(d)] we observe similar behaviors for time delays longer than ~2 ps, while immediately after excitation we observe a distorted signal due to the Stark effect [37]. Also for pump photon energy lower than the CdS band gap (at 510 nm), Fig. 2(g), we detect a positive PB of CdS shell, with fast rise time (<300 fs) and similar subsequent behavior as above. This last case represents a clear indication of a quasi-type-II band alignment, with electrons delocalized all over the structure. In the last case, we photogenerate excitons only in the core but we detect a PB signal from the shell; it can happen only if excited electrons are delocalized in the shell, given the high mismatch of the valence band of PbS and CdS. These findings are consistent with the presence of PL emission from CdS states.

In core/GSS NCs, transient spectra reveal a very complex situation. Pumping at the band edge (pump wavelength at 470 nm) for small $\langle N \rangle$ values [Fig. 2(b)], we observe the instantaneous formation of a positive peak at around 461 nm corresponding to the negative peak of the second derivative of the linear absorption spectrum; since the absorption of core/GSS NCs is dominated by the absorption of the CdS shell in the Wz phase, we ascribe this peak to the PB of the Wz-CdS band gap. A second positive peak appears in the transient spectrum [Fig. 2(b)] at long probe wavelengths, which redshifts in time becoming stable in ~1 ps [see also Fig. 3(b)]. This is a second PB signal, which is due to the Zb-CdS band gap transition [22]. The temporal evolution of the energy of this peak is due to the relaxation of the strong electric field of core excitons, likewise the Stark effect. The two PB peaks show different time evolution in the first picosecond, with the Wz PB decaying and the Zb PB growing in time, denoting an electron redistribution between the CdS states [Figs. 3(b), 3(e), and S4(a)]. At longer time delay both PBs have a long-living signal, with a time constant of ~3 ns associated with exciton recombination in the CdS shell [22]. Also with the pump tuned at high photon energy, at 400 nm, we observe the two PBs ascribed to the two CdS crystal structures and the same fast electron redistribution in the first picosecond [Fig. S4(c)]. Before the formation of the Zb-CdS PB, an initial negative signal (photoinduced absorption, PA) at larger probe wavelengths is observed due to the Stark effect. For low pump photon energy (at 510 nm) we still observe two PBs [Fig. 2(h)]; however, in this case, the amplitude of the PB associated with the Wz-CdS band gap is much lower than the amplitude of the Zb-CdS PB. This is probably due to direct excitation of Zb-CdS. Here again we can infer that electrons are delocalized and that the sample has a good quality with no defects, which would have caused long-living PAs. The data allow us to draw the band structure scheme. The bulk energy band gaps of PbS, Zb-CdS, and Wz-CdS are respectively 3 μm [38], 496 nm, and 488 nm [39]. PbS has symmetric energy structure because of equivalent electron and hole effective masses $m_h^* = m_e^* = 0.085 m_0$ (Ref. [40]) while CdS has $m_h^* = 0.7 m_0$ and $m_e^* = 0.2 m_0$ (Ref. [41]) for holes

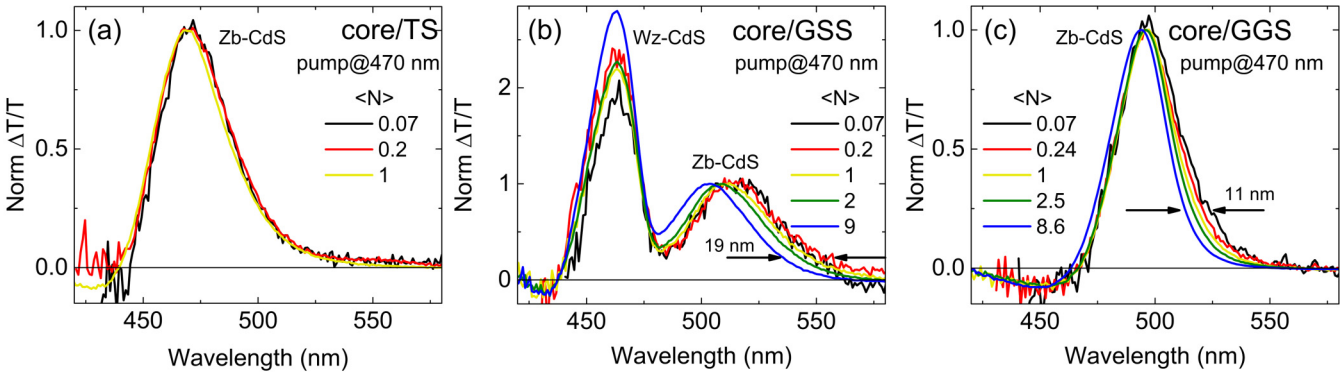

FIG. 4. Normalized $\Delta T/T$ spectra at 750 ps time delay for various $\langle N \rangle$ for (a) core/TS, (b) core/GSS, and (c) core/GGS NCs pumped at 470 nm. The line displacements are calculated at 25% of the peak height.

and electrons, respectively, indicating with m_0 the electron mass at rest in vacuum. Taking into account the quasi-type-II alignment discussed above, we can enlarge the bulk energy band gaps proportionally to the effective masses. The final scheme of band alignment of core/GSS NCs is shown in Fig. 3(d). Altogether, these results show the excited-state behavior and evolution and demonstrate the possibility of obtaining radiative emission from shell states.

In core/GGS NCs, by pumping at the band edge at 470 nm for small $\langle N \rangle$ values [Fig. 2(c)] we observe an instantaneous formation of a positive signal that initially presents the two distinct PB peaks (at about 479 and 496 nm) due to Wz-CdS and Zb-CdS, while at longer time delays a broad negative band appears, for wavelengths lower than about 470 nm, leaving a single positive peak at around 496 nm. The negative band of PA forms in a few hundred femtoseconds (∼500 fs) and has a long-living signal [Fig. 3(f)], which overcomes the PB in the blue side at long time delays; we assign it to trap states because of its long lifetime [42] and shape [43]. The fast disappearance of the Wz-CdS PB can also be related to a relaxation of excitons from the CdS shell to the PbS core assisted by the graded core/shell interface. Also in this sample, the PB at 496 nm has a long-living signal [Fig. 3(c)] with a time constant of ∼3 ns associated with exciton recombination in the CdS shell [22]. Pumping with high-energy photons at 400 nm [Fig. 2(f)] we observe the derivative feature associated with the Stark effect immediately after excitation and the peak at 496 nm after the first picosecond in $\Delta T/T$ spectra. Even for low pump photon energy (510 nm) we could still detect the positive PB of the CdS shell, even if partially overcome by the PA band. Here again, we can conclude that the electrons are delocalized. Finally, the negative signal at low wavelengths in $\Delta T/T$ spectra [Figs. 2(c), 2(f), and 2(i)] has a weight, relative to the PB peak, that increases with decrease of the pump photon energy [see also Fig. 3(f), in which the signals have been normalized to the peak of the PB band]. This indicates that trap states are correlated to defects at the interface between core and shell, which can be circumvented by proper choice of the pump wavelength. The band alignment that we expect for this sample is as the one of core/GSS NCs [Fig. 3(d)] but with a graded interface between the PbS core and the Zb-CdS shell. Here again the data indicate the band alignment and the excited-state behavior.

We also recorded $\Delta T/T$ dynamics for different pump fluences. In Figs. 3(a)–3(c) and 3(e), we plot the results on a long time scale (750 ps) for the pump tuned at 470 nm (CdS band edge), to discard possible effects due to higher energy states [42]. In core/TS NCs [Fig. 3(a)], the decay becomes faster by increasing the number of excitons per dot. The dynamics can be fitted by a biexponential function convolved with the instrumental function; for $\langle N \rangle = 0.2$ the first time constant is about 110 ps and the second one 3–4 ns; for $\langle N \rangle = 1$ the first time constant decreases to ∼50 ps, consistently with an Auger recombination process, which is very effective yet for $\langle N \rangle$ close to 1 (i.e., when only a small fraction of NCs has more than one exciton, according to the theoretical Poisson distribution, plotted in Fig. S5 in the SM [27]). Interestingly in core/GSS NCs and in core/GGS NCs, the time evolution of PB is hardly affected by the number of excitons [Figs. 3(b), 3(c), and 3(e)], thus confirming that Auger decay is barely effective even for high occupancies, in particular for the core/GGS case; this is consistent with what is observed in PL measurements. However, in all three kinds of NCs, shell electrons are long living also at high pump fluences, and can therefore give rise to PL emission from CdS, yet the different dynamics confirm a decoupling of core and shell excitons in core/GSS and core/GGS NCs.

When increasing the pump fluence, and thus $\langle N \rangle$, we observe further peculiar features in $\Delta T/T$ data in core/GSS and core/GGS NCs. At very high fluences, the initial electron redistribution in CdS cannot be observed (Figs. S4(b) and S4(d) in the SM [27]); moreover pumping at the CdS band edge (470 nm), the PB is formed instantaneously (faster than the time resolution of our apparatus) (Fig. S4(b) in the SM [27]), while pumping at high photon energy (400 nm) PB is formed in about 1 ps (Fig. S4(d) in the SM [27]) due to thermalization of high-energy excitons. By tuning the pump at 470 nm, we observe a slowdown in the decay, which excludes the possibility of biexciton effects that would instead lead to an opposite behavior [31]. Furthermore pumping at 400 nm and at 470 nm we observe a blueshift of the PB peak associated with Zb-CdS when $\langle N \rangle$ increases. In Figs. 4(b) and 4(c) we plot the $\Delta T/T$ spectra recorded at long time delays (750 ps) for various excitation fluences (exciting at 470 nm) for core/GSS and core/GGS NCs. In particular in core/GSS NCs this blueshift is accompanied by an increase of the height of the Wz-CdS PB band (at around 461 nm). In Fig. S6 we plot the ratio between the heights of the CdS PB bands, which is related to the state populations, and the peak position of the Zb-CdS

peak as a function of $\langle N \rangle$ and we observe a very similar trend which indicates a strict relation between these two quantities. In core/GGS NCs, this effect, even if hidden by the PA of traps in the blue part of the spectrum, can be clearly noticed in the red part [Fig. 4(c)]. The same blueshift in core/GSS and core/GGS NCs can be observed pumping with high-energy photons at 400 nm (Fig. S7 in the SM [27]). Conversely the shift is negligible in core/TS NCs [Fig. 4(a)]. We highlight that the blueshift of the Zb-CdS PB cannot be ascribed to state filling of higher energy states (Burnstein-Moss effect), because in this case the PB spectrum should broaden, keeping its red side unperturbed [44,45]. These phenomena instead interestingly indicate that the Zb-CdS band gap enlarges by increasing $\langle N \rangle$ in giant NCs. This leads to an increasing barrier between the core and Wz-CdS shell, which prevents the relaxation of Wz-CdS excitons and consequently results in a growing role of Wz-CdS excitons in the transient transmission data. The enlargement of the Zb-CdS band gap is associated with an increase of the electrostatic repulsion among holes in the small core and holes in the CdS shell [16]. These data thus describe completely the dynamic hole blockade effect that results in decoupling of core and shell excitons. Moreover they show that this phenomenon affects all giant shell NCs, independently of the core/shell interface, and has no role in core/TS NCs.

The overall data highlight that core/TS, core/GSS, and core/GGS NCs show a quasi-type-II band alignment in which electrons are delocalized with a very long decay time. This allows radiative recombination in the CdS shell, together with core radiative recombination, resulting in simultaneous dual emission, also in NCs, with thin shell. Beyond this similarity, we also highlight the differences. In core/TS NCs the reduced volume of the particle leads to strictly connected core and shell excitons and to a quite effective nonradiative Auger recombination process. The large volume of giant NCs can overcome these effects, decoupling core and shell excitons and drastically reducing the nonradiative Auger effect, in particular in NCs with alloyed core/shell interface. A very interesting result regards the enlargement of the Zb-CdS barrier due to the electrostatic repulsion of holes in the core in giant NCs, for both sharp and graded interfaces, which depends on the number of excitons in the NC. This dynamic barrier, which we observe in detail, facilitates the emission from the CdS shell in both giant NCs, yet results in better performances in alloyed interfaces. These findings give a rationale to the role of the shell volume and of the core/shell interface and thus provide a further insight into the physics of dual emission so far reported in the literature. All dual-emitting NCs described in the literature are characterized by a large volume of the shell [2,16,19,20,22,23] or of part of the structures, like the pods in tetrapods [12–14,17], or the rod shell in dot/rod NCs [12,15], in agreement with our conclusions. Here, in addition, we provide information on the role of the core/shell interface in exciton relaxation and describe the dynamical physical processes and the excited-state evolution as a function of time and excitation conditions.

D. Amplified spontaneous emission

A further important feature of NCs is related to the possibility of obtaining optical gain. We prepared films of core/TS, core/GSS, and core/GGS samples, thick enough to allow wave guiding at 500 nm. The films were excited by 100-fs laser pulses at 400 nm incident at 45° to the sample, focused on a rectangular spot of 1.79×0.09 mm^2, and emission was collected normally to the substrate (to avoid collection of leaky modes [46] by the fiber-coupled spectrometer). Using the film of core/TS and core/GSS NCs we obtained PL spectra analogous to those shown in Figs. 1(a) and 1(b). Shining a film made of core/GGS NCs we obtained spectra similar to that of Fig. 1(c) when pumping at low fluences, while at high pump fluences, higher than a certain value, the CdS band showed a clear line narrowing accompanied by a change in the slope of the input-output characteristics, as reported in Fig. 5. These are clear signatures of a process of amplified spontaneous emission (ASE). This marks a further difference between core/GSS and core/GGS NCs, dictated by the core/shell interface. These observations denote that core/GGS NCs sustain optical gain due to the large shell volume and a better suppression of Auger recombination and can thus be used as amplifiers or for laser applications.

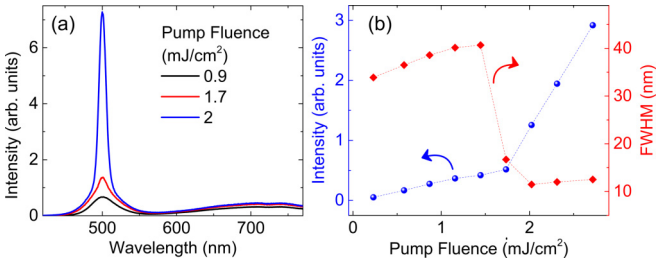

FIG. 5. (a) Emission spectra of the core/GGS NC film at different pump fluences and (b) emission intensity (blue spheres) and full width at half maximum (red diamonds) vs pump fluence, pumping at 400 nm.

III. CONCLUSIONS AND PERSPECTIVES

In conclusion, we studied PbS/CdS NCs obtained by cation exchange, followed by SILAR, with sharp and alloyed interface between PbS and CdS, and different shell thicknesses. We found that they have a quasi-type-II band alignment and can give rise to dual simultaneous emission originating from core and shell states, independently of the thickness of the shell (i.e., also in NCs with thin quantum-confined shell) and of the core/shell interface. Nevertheless, while the core PL emission behavior is affected to a small extent by the shell characteristics, the shell PL signal is greatly influenced by the shell thickness and by the core/shell interface. In addition the ratio between the intensities of shell and core PL signals depends on both shell thickness and core/shell interface. Shell PL is weaker than core PL in core/TS NCs, is stronger in core/GSS NCs, and depends on the pump fluence in core/GGS NCs (being weaker or stronger for low or high pump fluences, respectively). We investigated the fast exciton dynamics and described the physics of exciton relaxation, elucidating the process responsible for shell PL. We showed the coupling and decoupling of core and shell excitons. We describe the coupling, and the quite effective Auger recombination process, due to the thin shell. On the other hand we show how the large shell volume and the interface barrier allow decoupling of core and shell excitons. We studied the dynamic behavior

of the interface barrier of the CdS in the zinc-blende phase, which is placed between the core and the outer CdS wurtzite shell. We showed the evolution of the dynamic hole barrier in detail and its effect on the decoupling between core and shell excitons. The decoupling allows an efficient shell PL for giant NCs with both sharp and graded interface, especially at high pump fluences in this last case. Last, but not least, we found that the core-shell exciton decoupling in core/GGS NCs enables the achievement of optical gain. All these findings are of great relevance for an exhaustive analysis of dual-emitting NCs, and allow a comprehensive understanding of the physics of single or dual emission in core/shell NCs, highlighting the role of the shell volume and of the core/shell interface. They will also facilitate the engineering of dual-emitting NCs, and ultimately the development of devices based on ratiometric fluorescence or other photonics applications.

ACKNOWLEDGMENTS

M.Z.-R. and A.C. acknowledge the project MIUR-PRIN 2015WTW7J3 (HotPlasMoS2), for financial support. G.S. and M.Z.-R. acknowledge COST Action MP1302-NanoSpectroscopy. A.V. acknowledges the Knut and Alice Wallenberg Foundation, the Swedish Foundations Consolidator Fellowship, the LTU Labfund program, and the Kempe Foundation for partial funding. A.V. acknowledges the European Commission for partial funding under the grants F-LIGHT (GA 299490) and WIROX (GA 295216). F.R. acknowledges partial salary support from the Canada Research Chairs program. F.R. is also grateful to the Government of China for a short-term Chang Jiang scholar award and to Sichuan province for a 1000 talent short-term award.

[1] P. V. Kamat and G. D. Scholes, J. Phys. Chem. Lett. **7**, 584 (2016).
[2] H. Zhao, A. Vomiero, and F. Rosei, Small **11**, 5741 (2015).
[3] E. J. McLaurin, L. R. Bradshaw, and D. R. Gamelin, Chem. Mater. **25**, 1283 (2013).
[4] C. Wang, S. Zhou, S. Xu, Z. Wang, and Y. Cui, Nanotechnology **25**, 375602 (2014).
[5] S. K. Panda, S. G. Hickey, H. V. Demir, and A. Eychmller, Angew. Chem. Int. Ed. **50**, 4432 (2011).
[6] S. Sapra, S. Mayilo, T. A. Klar, A. L. Rogach, and J. Feldmann, Adv. Mater. **19**, 569 (2007).
[7] L. Peng, D. Li, Z. Zhang, K. Huang, Y. Zhang, Z. Shi, R. Xie, and W. Yang, Nano Res. **8**, 3316 (2015).
[8] V. A. Vlaskin, N. Janssen, J. van Rijssel, R. Beaulac, and D. R. Gamelin, Nano Lett. **10**, 3670 (2010).
[9] Z. Zhang, D. Liu, D. Li, K. Huang, Y. Zhang, Z. Shi, R. Xie, M.-Y. Han, Y. Wang, and W. Yang, Chem. Mater. **27**, 1405 (2015).
[10] G. Huang, C. Wang, S. Xu, Z. Qi, C. Lu, and Y. Cui, Nanotechnology **27**, 185602 (2016).
[11] E. A. Dias, A. F. Grimes, D. S. English, and P. Kambhampati, J. Phys. Chem. C **112**, 37 (2008).
[12] A. A. Lutich, C. Mauser, E. Da Como, J. Huang, A. Vaneski, D. V. Talapin, A. L. Rogach, and J. Feldmann, Nano Lett. **10**, 4646 (2010).
[13] N. J. Borys, M. J. Walter, J. Huang, D. V. Talapin, and J. M. Lupton, Science **330**, 1371 (2010).
[14] C. L. Choi, H. Li, A. C. K. Olson, P. K. Jain, S. Sivasankar, and A. P. Alivisatos, Nano Lett. **11**, 2358 (2011).
[15] R. Krahne, M. Zavelani-Rossi, M. G. Lupo, L. Manna, and G. Lanzani, Appl. Phys. Lett. **98**, 063105 (2011).
[16] C. Galland, S. Brovelli, W. K. Bae, L. A. Padilha, F. Meinardi, and V. I. Klimov, Nano Lett. **13**, 321 (2013).
[17] J. I. Wong, N. Mishra, G. Xing, M. Li, S. Chakrabortty, T. Chien Sum, Y. Shi, Y. Chan, and H. Y. Yang, ACS Nano **8**, 2873 (2014).
[18] W.-Y. Wu, M. Li, J. Lian, X. Wu, E. K. L. Yeow, M. H. Jhon, and Y. Chan, ACS Nano **9**, 9349 (2014).
[19] H. Zhao, H. Liang, B. A. Gonfa, M. Chaker, T. Ozaki, P. Tijssen, F. Vidal, and D. Ma, Nanoscale **6**, 215 (2014).
[20] C. Liao, K. Fan, R. Xu, H. Zhang, C. Lu, Y. Cui, and J. Zhang, Photon. Res. **3**, 200 (2015).
[21] S. Liu, N. J. Borys, S. Sapra, A. Eychmìller, and J. M. Lupton, Chem. Phys. Chem. **16**, 1663 (2015).
[22] H. Zhao, G. Sirigu, A. Parisini, A. Camellini, G. Nicotra, F. Rosei, V. Morandi, M. Zavelani-Rossi, and A. Vomiero, Nanoscale **8**, 4217 (2016).
[23] V. Pinchetti, F. Meinardi, A. Camellini, G. Sirigu, S. Christodoulou, W. K. Bae, F. De Donato, L. Manna, M. Zavelani-Rossi, I. Moreels, V. I. Klimov, and S. Brovelli, ACS Nano **10**, 6877 (2016).
[24] M. Zavelani-Rossi, M. G. Lupo, F. Tassone, L. Manna, and G. Lanzani, Nano Lett. **10**, 3142 (2010).
[25] L. Jin, G. Sirigu, X. Tong, A. Camellini, A. Parisini, G. Nicotra, C. Spinella, H. Zhao, S. Sun, V. Morandi, M. Zavelani-Rossi, F. Rosei, and A. Vomiero, Nano Energy **30**, 531 (2016).
[26] M. Zavelani-Rossi, R. Krahne, G. Della Valle, S. Longhi, I. R. Franchini, S. Girardo, F. Scotognella, D. Pisignano, L. Manna, G. Lanzani, and F. Tassone, Laser Photon. Rev. **6**, 678 (2012).
[27] See Supplemental Material at http://link.aps.org/supplemental/10.1103/PhysRevB.96.155303 for further figures and description of the synthesis of the Pbs/CdS NCs.
[28] M. Saba, S. Minniberger, F. Quochi, J. Roither, M. Marceddu, A. Gocalinska, M. V. Kovalenko, D. V. Talapin, W. Heiss, A. Mura, and G. Bongiovanni, Adv. Mater. **21**, 4942 (2009).
[29] Y.-S. Park, A. V. Malko, J. Vela, Y. Chen, Y. Ghosh, F. García-Santamaría, J. A. Hollingsworth, V. I. Klimov, and H. Htoon, Phys. Rev. Lett. **106**, 187401 (2011).
[30] E. Istrate, S. Hoogland, V. Sukhovatkin, L. Levina, S. Myrskog, P. W. E. Smith, and E. H. Sargent, J. Phys. Chem. B **112**, 2757 (2008).
[31] V. I. Klimov, A. A. Mikhailovsky, W. McBranch, C. A. Leatherdale, and M. G. Bawendi, Science **287**, 1011 (2000).
[32] G. E. Cragg and A. L. Efros, Nano Lett. **10**, 313 (2010).
[33] M. Achermann, J. A. Hollingsworth, and V. I. Klimov, Phys. Rev. B **68**, 245302 (2003).
[34] V. I. Klimov, S, A. Ivanov, J. Nanda, M. Achermann, I. Bezel, J. A. McGuire, and A. Piryatinski, Nature (London) **447**, 441 (2007).
[35] F. García-Santamaría, S. Brovelli, R. Viswanatha, J. A. Hollingsworth, H. Htoon, S. A. Crooker, and V. I. Klimov, Nano Lett. **11**, 687 (2011).

[36] V. I. Klimov, J. Phys. Chem. B **104**, 6112 (2000).
[37] D. J. Norris, A. Sacra, C. B. Murray, and M. G. Bawendi, Phys. Rev. Lett. **72**, 2612 (1994).
[38] Y. Wang, A. Suna, W. Mahler, and R. Kasowski, J. Chem. Phys. **87**, 7315 (1987).
[39] Z. Z. Bandíc and Z. Ikonić, Phys. Rev. B **51**, 9806 (1995).
[40] P. Amirtharaj and D. G. Seiler, in *Handbook of Optics*, edited by M. Bass *et al.* (McGraw-Hill, New York, 1995), Vol. 2, Chap. 36.
[41] J. W. Haus, H. S. Zhou, I. Honma, and H. Komiyama, Phys. Rev. B **47**, 1359 (1993).
[42] P. Kambhampati, J. Phys. Chem. C **115**, 22089 (2011).
[43] P. Tyagi and P. Kambhampati, J. Chem. Phys. **134**, 094706 (2011).
[44] H. Zhu, N. Song, W. Rodríguez-Córdoba, and T. Lian, J. Am. Chem. Soc. **134**, 4250 (2012).
[45] J. S. Manser and P. V. Kamat, Nat. Photon. **8**, 737 (2014).
[46] D. Marcuse, *Theory of Dielectric Optical Waveguides* (Academic Press, New York, 1974).